New Perspectives on Supercritical Methane Adsorption in Shales and Associated Thermodynamics

Xu Tang[1,2], Nino Ripepi[3], Sean Rigby[4], Robert Mokaya[1], Ellen Gilliland[3]

1. School of Chemistry, University of Nottingham, Nottingham, NG7 2RD, UK;
2. Key Laboratory of Petroleum Resources Research, Institute of Geology and Geophysics, Chinese Academy of Sciences, Beijing 100029, China;
3. Department of Mining and Minerals Engineering, Virginia Polytechnic Institute and State University, Blacksburg, Virginia 24060, United States;
4. Department of Chemical and Environmental Engineering, University of Nottingham, Nottingham, NG7 2RD, UK.

Highlights:

- A rigorous framework is applied to interpret methane adsorption behavior in shales.

- Adsorption isotherms under different pressures and temperatures can be represented by a 2D surface.

- Adsorbed methane density in shales is a function of pressure and temperature.

- Maximum adsorption uptake of shales is independent of temperature and pressure.

- Isosteric enthalpy and entropy depend on surface coverage and temperature.

Abstract: Understanding methane adsorption behavior in shales is fundamental for optimizing shale gas development as the adsorbed methane is a large portion of the subsurface shale gas resource. However, the adsorption mechanism of supercritical methane in shales and associated thermodynamics are poorly understood because the equation of state of the adsorbed methane is unmeasurable. This work analyzed adsorption equilibria (up to 32 MPa and 393.15 K) using a rigorous framework that can account for non-ideal gas properties and accurately extrapolate absolute adsorption uptakes from measured adsorption isotherms. The framework also allows a straightforward calculation of thermodynamic potentials relevant to adsorption such as enthalpy and entropy. Modelling results show that methane adsorption isotherms in shale under different pressures and temperatures are represented by a two dimensional adsorption isotherm surface. The density of the adsorbed methane in shales depends on temperature and pressure, which is always lower than the liquid methane density but higher than the corresponding gaseous methane density. The temperature-dependent and pressure-dependent characteristics of adsorbed methane density leads to the corresponding temperature-dependent and pressure-dependent measured/absolute adsorption isotherms. The maximum adsorption uptake of shales is independent of temperature and pressure. The isosteric enthalpy/entropy of adsorption and enthalpy/entropy of adsorbed methane are found to be temperature- and surface coverage-dependent. These new findings therefore not only clarify some historical misunderstandings of methane adsorption in shales for engineering application, but also provide a novel framework for interpreting methane adsorption behavior in shales and for determining the associated thermodynamics.

Key words: Shale, Methane, Adsorption, Enthalpy, Adsorbed density

1 Introduction

Natural gas produced from subsurface shale formations, also called shale gas, has changed world energy supplies and continues to have global implications for a low carbon-constraint economy. A U.S. Energy Information Administration (EIA) study indicates that shale gas is expected to account for 30% of the global natural gas production by 2040 (International Energy Outlook 2016). According to the EIA report, there are 35,782 Trillion cubic feet (Tcf) of risked shale gas in-place across 41 countries, of which 7299 Tcf shale gas is considered technically recoverable. With the advancement of hydraulic fracturing and horizontal drilling technologies, producing shale gas from subsurface formations is becoming economically feasible. The U.S. was the first country to produce commercial volumes of shale gas, followed by Canada, China and Argentina. Extensive researches have been conducted to understand the nature of existing shale gas and their transport behavior in subsurface formations in order to estimate the total shale gas resource and the best manage production (Curtis, 2002; Jarvie et al., 2007; Ross et al., 2009; Kargbo et al., 2010; Civan et al., 2011). However, resource estimates involve significant uncertainties due to the complex behavior of shales as porous structures and must be treated with considerable caution (Loucks et al., 2009; Ambrose et al., 2010; Sondergeld et al., 2010; Slatt et al., 2011; Mcglade et al., 2013; Chen et al., 2017; Striolo et al., 2017). An improved understanding of the behavior of methane in subsurface shale formations is therefore critical in order to optimize the development of shale gas resources.

Shale gas, consisting mainly of methane, exists in three different states at subsurface shale formations: adsorbed phase that is weakly bounded to the pore surfaces, bulk phase in the free pore space excluding the space occupied by adsorbed phase, and a small amount of dissolved phase in organic matter and formation liquids. Previous studies have revealed that adsorbed methane accounts for 30%-80% of total gas reservoirs (Curtis, 2002). Since most shale formations are in high pressure and temperature (up to 27 MPa and 360 K) reservoir conditions, shale gases are usually under supercritical conditions because the critical point of methane is 190.4 K and 4.6 MPa. It is also well-known that the physical properties of supercritical gas are different from its subcritical status because distinct liquid and gas phases do not exist for supercritical fluids (McHugh et al., 2013). This specific property not only distinguishes the adsorption behavior of supercritical gas from subcritical gas, but also challenges the description and interpretation of methane adsorption behavior in shales (Tang et al., 2016a). However, description of the supercritical methane adsorption behavior in shales still follows the subcritical gas adsorption theory wherein the density of the adsorbed phase is assumed to be equal to the liquid density or quasi-liquid density. Since estimating the shale gas in place resource is the very first step for shale gas development, there is an urgent need to understand the real nature of supercritical methane adsorption in shales. Such an understanding is critical as it will lay the foundation for developing a reasonable gas transport model in shales and understanding of the associated heat transfer process during shale gas production (Ambrose et al., 2010; Civan et al., 2011; Akkutlu et al., 2012).

Accurate estimation of adsorbed methane content in shales under supercritical conditions (subsurface reservoir conditions) still remains unclear. Accurate extrapolation of the absolute (true) adsorption uptake from measured adsorption isotherms requires a thorough understanding of the equation of states (EOS) of the adsorbed phase, i.e., how the volume or density of the adsorbed phase changes with temperature and pressure (Tang et al, 2017b). However, the EOS of the adsorbed methane is yet to be established as it cannot be directly measured using current technologies. Different researchers thus apply a variety of assumptions to interpret the mechanism of supercritical methane adsorption in shales. Experimentalists in unconventional gas industry adopt the historical idea that the density of the adsorbed methane in shale can be treated as liquid or quasi-liquid, and that the quasi-liquid density of methane is larger than the

corresponding gaseous phase density but lower than the liquid density (Weniger et al., 2010; Gasparik et al., 2012 & 2015; Gensterblum et al., 2013; Clarkson et al., 2013; Yang et al., 2105; Tang et al., 2016, 2017a, 2017b & 2017c; Tian et al., 2016; Zhou et al., 2018; Li et al., 2018a; Shabani et al, 2018; Li et al., 2018b; Hu et al, 2018). This assumption is valid for subcritical gas adsorption in micropore (<2 nm) rich porous materials due to the nanoconfinement effect. The pore filling model is now routinely for characterizing micropores in porous media based on the potential theory of Polanyi (Dubinin, 1965, 1960 & 1971; Thommes et al., 2015). The model, however, becomes invalid as the adsorbate changes from subcritical gas to supercritical fluid because distinct liquid and gas phases do not exist for supercritical fluids and the pore filling mechanism is no longer valid for mesopores (2-50 nm) and macropores (> 50 nm). Shale gas in deep subsurface reservoirs usually exist in supercritical fluid form. Some abnormal values of the quasi-liquid density of methane have been reported that are higher than the liquid methane density (Tian et al., 2016; Rexer et al., 2013; Hu et al., 2018; Zhou et al., 2018). On the other hand, according to molecular dynamics simulation, models show that the density of the adsorbed phase of supercritical fluid depends on both temperature and pressure in mesopores and macropores and is not constant, and that the adsorbed phase in micropores follows pore filling theory (Ambrose et al., 2010; Xiong et al., 2016; Tian et al., 2017; Zhang et al., 2014 & 2016; Liu et al., 2018; Li et al., 2014; Jin et al, 2013 & 2016; Zhu et al., 2014; Wu et al., 2015; Zhao et al., 2018; Wang et al, 2018). The density of the adsorbed phase increases with increasing pressure, and decreases with increasing temperature and thus follows a Langmuir-style trend while the location and thickness of the adsorbed layer remains constant (Zhang et al., 2014; Zhu et al., 2014; Tian et al., 2017; Liu et al., 2018). Even though these insights have been adopted by some experimentalists to interpret the supercritical gas adsorption in shales, the corresponding thermodynamic characteristics have rarely been studied (Bae et al., 2006; Sakurovs et al., 2007; Rexer et al., 2013; Pini et al., 2010). Furthermore, the powerful molecular simulation approach has not been widely adopted in the unconventional gas industry because of high computing costs and the simplified and unrealistic model cannot mimic the realistic pore structure and surface chemical properties of shales. The historical debates between experimentalists and modelers also impede the true understanding of supercritical methane and shale interaction under reservoir conditions and the correct understanding of shale gas flow in shales. Therefore, a new phenomenological model that settles the dispute between experimentalists and modelers by adopting molecular insights is urgently needed to allow interpretation of supercritical methane adsorption behavior in shale.

Analysis of the thermodynamics (e.g., enthalpy and entropy) of supercritical methane adsorption in shales can reveal important information about methane-shale interactions. For example, when the isosteric enthalpy is lower than 40 kJ/mol, the interaction can be treated as physical adsorption. Changes in the isosteric entropy reveal the mobility of the adsorbed phase. Even though researchers have investigated isosteric enthalpy (historically called isosteric heat) for supercritical methane in shales, their methods are not accurate because they use a simplified form of the Clausius–Clapeyron (C-C) equation (Zhang et al., 2012; Gasparik et al., 2012; Rexer et al., 2013; Ji et al., 2015; Yang et al., 2015; Tian et al., 2016; Zou et al., 2017; Shabani et al., 2018; Li et al., 2018a; Li et al., 2018b). The simplified form of the C-C equation assumes that gas obeys the ideal gas law and the volume of the adsorbed phase is neglected (Huang et al., 1972; Pan et al., 1998; Chakraborty et al., 2006). This is true for subcritical gas under low pressure condition but is invalid for supercritical gas as behavior deviates significantly from the ideal gas law, and the effect of the adsorbed phase volume becomes even more pronounced. The simplified form of the C-C equation cannot show the temperature dependent behavior of the isosteric enthalpy of adsorption, which has been observed from calorimetry and temperature measurement (Cao et al., 2001; Yue et al., 2015). Furthermore, it is difficult to set up a thermodynamically standard state for the adsorbed phase of supercritical gas. The standard state usually refers to

the liquid-like state of gas for subcritical gas adsorption processes, however, this assumption is not valid for supercritical fluids (Zhou et al, 2000a & 2000b; Zhou et al., 2009). Moreover, using the liquid methane density or quasi-liquid density to extrapolate the absolute adsorption uptake from directly measured data is questionable even though previous works assert that the assumption allows researchers to investigate adsorption thermodynamics by considering both real gas behavior and the effect of adsorbed phase (Mertens et al., 2009; Stadie et al., 2013; Stadie et al., 2015; Tang et al., 2017a, 2017b & 2017c; Murialdo et al., 2018). As mentioned earlier, the liquid methane density or quasi-liquid assumption contradicts molecular dynamics simulations where adsorbed density is a function of pressure and temperature. Whether the dynamic adsorbed density can reveal the realistic thermodynamic characteristics of supercritical methane in shales still needs to be validated. Therefore, a rigorous and physically consistent approach for investigating the surface thermodynamic properties such as enthalpy and entropy by analyzing experimental adsorption equilibria using molecular dynamics insights is urgently needed. This will also lay the foundation for developing enhanced shale gas recovery technology by using thermal stimulation approaches.

This report first presents an alternative framework for analyzing measured supercritical methane adsorption equilibria including adsorption model and the analytical method of calculating enthalpy and entropy of adsorption. Secondly, our proposed approach is used for analyzing supercritical methane adsorption equilibria of four different shales from literature (19 adsorption isotherms with 350 measured points at pressures up to 32 MPa and temperatures up to 393.15 K). The adsorption isotherm characteristics, the adsorbed methane density, and thermodynamic properties are discussed in details. Lastly, the model resulting from the proposed framework is compared with two routinely used methods from the literature.

2 Supercritical gas adsorption theory

Supercritical gas adsorption model. Supercritical gas adsorption in porous media is different from subcritical gas adsorption because assumptions such as multilayer formation, capillary condensation in small pores, and saturation pressure are not applicable for the supercritical fluid (Zhou et al, 2000a & 2000b; Do et al., 2003; Zhou et al., 2009; McHugh et al., 2013). Four basic assumptions are made here in order to develop a novel supercritical gas adsorption model for porous media,

(1) The porous media has a rigid structure;
(2) The absolute adsorption uptake of supercritical gas in porous media monotonously increases with increasing gas pressure;
(3) The intrinsic adsorption capacity of a heterogeneous porous framework is determined by material properties such as pore structure and surface chemistry;
(4) The location and thickness of the adsorbed layer remain constant and are determined by gas molecule-pore wall interaction.

The first assumption assumes the pore structure does not change during adsorption, and that adsorption induced deformation is beyond the scope of this work (Gor et al., 2017). The second assumption is well-known and has been validated by many researchers (Zhou et al, 2000a & 2000b; Murata et al., 2001; Mertens et al., 2009; Do et al., 2003; Thommes et al., 2015). For the third assumption, the intrinsic adsorption capacity refers to the limiting adsorption uptake under limiting pressure, which is determined by pore structure, surface chemistry of the pore and molecular size of the adsorbate (Zhou et al., 2009). The intrinsic adsorption capacity should not be confused with the measured adsorption uptake. Experimental observations show that the measured adsorption uptake depends on both pressure and temperature. The reason being that measured adsorption uptake is determined by the density and volume of the adsorbed phase and the adsorbed phase density changes with pressure and temperature, as shown in this work later.

The intrinsic adsorption capacity is historically referred to as the maximum adsorption uptake, and we will follow this tradition by using the maximum adsorption uptake in the following sections. These three assumptions are essentially similar to the corresponding assumptions of the classic Langmuir model; all adsorption sites on the surface are assumed to be equivalent and independent of each other, and that each site holds only one adsorbed molecule during adsorption and the total number of adsorption sites does not change (Langmuir, 1918). The fourth assumption is supported by molecular dynamics, where the interaction between an adsorbed molecule and a surface is described by the summation of pairwise 12-6 Lennard-Jones potential energies between the adsorbate molecule and all atoms of the surface (Ambrose et al., 2010; Xiong et al., 2016; Tian et al., 2017; Zhang et al., 2014 & 2016; Liu et al., 2018; Li et al., 2014; Jin et al, 2013 & 2016; Zhu et al., 2014; Wu et al., 2015; Zhao et al., 2018; Wang et al., 2017; Wang et al., 2019). For supercritical gas, a single adsorbed layer is considered to form an open surface where the adsorption potential between the adsorbate and the surface atoms is minimum (Do et al, 2003; Marmur, 2015; Tian et al., 2017; Liu et al, 2018). These has been evidenced by several Grand Canonical Monte Carlo Simulation (GCMS) studies, which indicate that supercritical methane adsorption in mesopores and macropores generally follows a single adsorbed layer and the thickness of the adsorbed layer approximates to the molecular diameter and is independent of pressure (Tian et al., 2017; Liu et al, 2018). For micropores, the adsorption forces are enhanced by overlapping of the adsorption potential from the opposite wall, which results in the pore filling phenomenon of supercritical adsorbate molecules (Do et al, 2003; Tian et al., 2017; Liu et al, 2018).

Following these four basic assumptions, a rigorous framework for modeling supercritical gas adsorption isotherms can be established using Gibbs excess adsorption theory. In any pure gas-solid adsorption system, the measured adsorption quantity, also called the Gibbs excess adsorption uptake (Gibbs, 1878), is shown by equation (1),

$$n_e = n_a - v_a \cdot \rho_g \qquad (1)$$

Where the excess adsorption quantity (n_e) refers to the difference between the absolute adsorption quantity (n_a) and the quantity of adsorbate that would be present in the same volume (v_a) of the adsorbed phase at the density of the bulk gas phase (ρ_g). Equation (1) can also be rewritten as,

$$n_e = v_a \cdot (\rho_a - \rho_g) \qquad (2)$$

Where ρ_a is the density of the adsorbed phase. According to equation (2), it can be concluded that negative measured adsorption quantity will appear only when the gas density is higher than the adsorbed phase density. However, the negative quantity cannot be observed from the GCMS study given that the adsorbed phase density is always higher than the bulk gas density up to 50 MPa (Tian et al., 2017). This, therefore, also means that any reported negative measured adsorption uptake can be attributed to experimental errors or inappropriate data processing methods (Ross et al., 2007; Zhang et al., 2016).

For real-world porous materials, a dual-site Langmuir model is applied to describe the absolute gas adsorption behavior by considering the material heterogeneity (Graham et al, 1953), as shown in equation (2),

$$n_a = n_{max} \cdot \left[(1-\alpha) \frac{K_1(T)P}{1 + K_1(T)P} + \alpha \frac{K_2(T)P}{1 + K_2(T)P} \right] \qquad (3)$$

Where n_{max} is the maximum adsorption uptake, while the energy of two different types of adsorption sites can be modelled by a separate equilibrium constant, $K_1(T)$ and $K_2(T)$ (

$K_1(T) = A_1 \cdot \exp(-\dfrac{E_1}{RT})$ and $K_2(T) = A_2 \cdot \exp(-\dfrac{E_2}{RT})$, A_1 and A_2 are pre-factors, E_1 and E_2 are adsorption

energies for different adsorption sites as determined by the gas and material properties) and weighted by a coefficient α (0<α<1), P is pressure, T is temperature, and R is the gas constant. It is worth emphasizing that n_{max} does not change with gas pressure and temperature.

By combining equation (1) and (3), equation (4) is obtained,

$$n_e = n_{max} \cdot \left[(1-\alpha)\frac{K_1(T)P}{1+K_1(T)P} + \alpha\frac{K_2(T)P}{1+K_2(T)P} \right] - v_a \cdot \rho_g \qquad (4)$$

If the adsorption volume, v_a, is an unknown constant, the density of the adsorbed phase can be easily calculated using equation (5),

$$\rho_a = \frac{n_a}{v_a} = \frac{n_{max}}{v_a} \cdot \left[(1-\alpha)\frac{K_1(T)P}{1+K_1(T)P} + \alpha\frac{K_2(T)P}{1+K_2(T)P} \right] \qquad (5)$$

It is expected that if equation (4) is used to fit measured adsorption isotherms under different pressures and temperatures, the volume of the adsorbed phase (v_a), the absolute adsorption uptake (equation 2) and the density of the adsorbed phase (equation 4) are readily available.

Isosteric enthalpy of adsorption. If the absolute adsorption uptake is available, the thermodynamic parameter, the isosteric enthalpy of adsorption (ΔH_{ads}), can be obtained. According to the Clausius–Clapeyron relationship (Clausius, 1850), the isosteric enthalpy in a closed gas adsorption system can be obtained by equation (6):

$$\Delta H_{ads} = (\frac{dP}{dT})_{n_a} \cdot T \cdot \Delta v = -(\frac{dP}{dT})_{n_a} \cdot T \cdot (v_a - \frac{1}{\rho_g}) \qquad (6)$$

The derivative of pressure with temperature along an isostere (constant value of adsorption uptake), $(\dfrac{dP}{dT})_{na}$, can be expanded into three simpler terms by introducing the surface coverage (θ) of a Langmuir style adsorption model using the Chain Rule in differentiating compositions of functions:

$$(\frac{dP}{dT})na = \left(\frac{dP}{dK}\right)_{na} \cdot \left(\frac{dK}{dT}\right)_{na} = \left(\frac{dP}{d\vartheta}\right)_{na} \cdot \left(\frac{d\vartheta}{dK}\right)_{na} \cdot \left(\frac{dK}{dT}\right)_{na} \qquad (7)$$

Where θ is surface coverage, the ratio of the absolute adsorption uptake (n_a) to the maximum adsorption uptake (n_{max}), $\theta = \dfrac{n_a}{n_{max}} = (1-\alpha)\dfrac{K_1(T)P}{1+K_1(T)P} + \alpha\dfrac{K_2(T)P}{1+K_2(T)P}$.

The analytical form of $(\dfrac{dP}{dT})_{na}$ in the case of the dual-site Langmuir equation (equation 3) is:

$$(\frac{dP}{dT})na = \frac{\frac{(1-\alpha)P}{(1+K_1(T)P)^2} \cdot \frac{-E_1 K_1(T)}{RT^2} + \frac{\alpha P}{(1+K_2(T)P)^2} \cdot \frac{-E_2 K_2(T)}{RT^2}}{\frac{(1-\alpha)K_1(T)}{(1+K_1(T)P)^2} + \frac{\alpha K_2(T)}{(1+K_2(T)P)^2}} \qquad (8)$$

If one ignores the volume of the adsorbed phase and applies the ideal gas law, equation (6) becomes the simplified C-C equation,

$$\Delta H_{ads} = (\frac{dP}{dT})_{n_a} \cdot T \cdot \Delta v = -(\frac{dP}{dT})_{n_a} \frac{RT^2}{P} \qquad (9)$$

Equation (6) has two advantages over equation (9). First, it incorporates non-ideal gas behavior. This is important because supercritical gas adsorption significantly deviates from subcritical gas adsorption. For methane, it deviates significantly at around 10 MPa and ambient temperature as attractive interactions become pronounced. As the pressure increases, the repulsive interactions gradually increase and become dominant. This is indicated by variation of the compressibility factor as shown in Figure 1; the compressibility factor is calculated by the modified Benedict–Webb–Rubin equation (BWR) equation of state as implemented in the REFPROP package (Lemmon et al., 2007). This deviation in behavior also means that methane density can be higher or lower than for an ideal gas at different pressures and temperatures. Second, equation (6) considers the volume of the adsorbed phase, which can be obtained by processing experimentally determined adsorption isotherms using equation (4) via a rigorous global fitting method (discussed in Section 3 below). Comparing equation (6) and (9), it is also clear that ignoring the volume of the adsorbed phase or applying the ideal gas law overestimates the calculated isosteric heat of adsorption for the gas adsorption system.
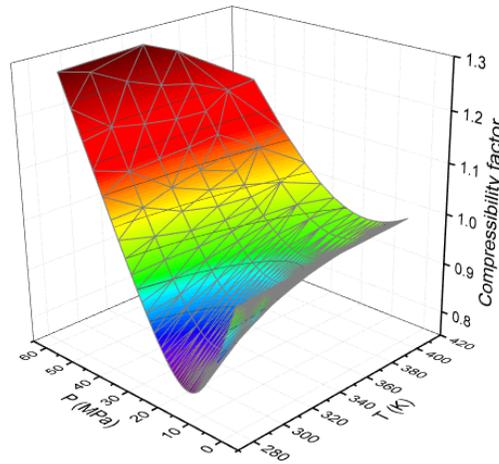

Figure 1. Compressibility factor of methane as a function of pressure and temperature.

Isosteric entropy of adsorption. The isosteric entropy of adsorption (ΔS_{ads}) and how it varies with surface coverage reveals the mobility of adsorbed phase (Tang, 2019). The isosteric entropy of adsorption refers to the change in entropy due to adsorption at a constant absolute adsorption uptake, and is readily defined by the Clausius–Clapeyron relationship:

$$\Delta S_{ads} = (\frac{dP}{dT})_{n_a} \cdot \Delta v = (\frac{dP}{dT})_{n_a} \cdot (v_a - \frac{1}{\rho_g}) \quad (10)$$

Comparing to equation (6), it is clear that ΔS_{ads} is readily available when ΔH_{ads} is known as shown in equation (11),

$$\Delta S_{ads} = \frac{\Delta H_{ads}}{T} \quad (11)$$

3. Data acquisition and processing

The supercritical methane adsorption isotherms in four different shales from China are directly retrieved from the literature. Samples FC-47, FC-66 and F-72 are collected at different depth from lower Cambrian shale formation in northeast Guizhou province and sample Longmaxi is from Longmaxi formation in Sichuan province (Li et al., 2017; Tang et al., 2016). The total organic carbon (TOC) of sample FC-47, FC-66, F-72 and Longmaxi is 3.5%, 7.3%, 11.3% and 4.52%, respectively, as measured using the gravimetric approach. All shale samples are dried to avoid moisture influence on the methane adsorption uptake. Detailed information about these samples, such as depth, mineralogical composition and pore structure, are referred to the original publications (Li et al., 2017; Tang et al., 2016), and therefore only the pertinent data are shown in **Figure 2**.
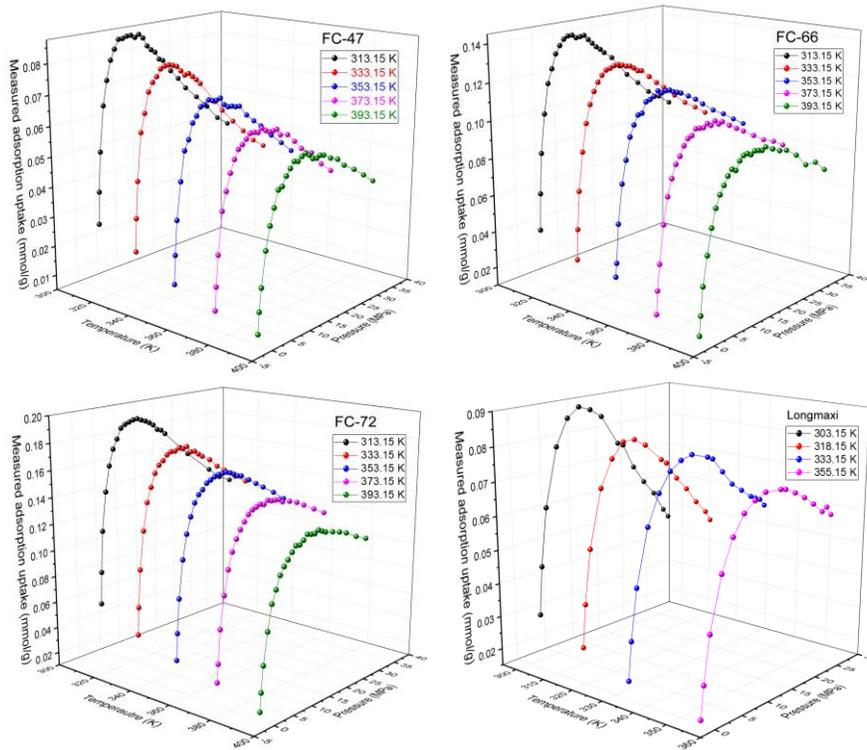

Figure 2 Supercritical methane adsorption isotherms in four different shales under elevated pressures and temperatures: experimental data retrieved from (Tang et al, 2016; Li et al., 2017), and the solid line is to connect data points for visualization.

The observed adsorption isotherms under different temperatures are fitted simultaneously using equation (4) within the limits of the fitting parameters ($0 < n_{max} < 100$ mmol/g, $0 < V_{max} < 100$ cm^3/g, $0 < \alpha < 1$, 5 kJ/mol $< E_1, E_2 < 100$ kJ/mol, $0 < A_1, A_2$). The test data is processed using the Universal Global Optimization (UGO) method of the Auto2Fit software (7D-soft High Technology Inc., China). The UGO can find the global maximum/minimal value of any functions without using the initial start values. This global fitting method also helps overcome the disadvantage of a graphical method, where the straight fitting line is not objectively determined (Pini, 2014). Once all fitting parameters (n_{max}, V_a, k, α, E_1, E_2, A_1 and A_2) are obtained from fitting the observed adsorption isotherms using equation (4), the absolute adsorption isotherms (equation 3), the adsorbed methane density (equation 5), the isosteric enthalpy (equation 6) and isosteric entropy (equation 10) are readily available.

Mathematically, equations (3, 4 and 5) represent two-dimensional surfaces as n_a, n_e and P_a are functions of two variables, P (pressure) and T (temperature). This also means that if the unknown parameters (n_{max}, V_a, k, α, E_1, E_2, A_1 and A_2) in equation (3) are obtained, the two-dimensional surfaces of n_a, n_e and p_a are readily available. Once the two-dimensional surfaces are known, methane adsorption isotherms beyond the available test data can be readily extrapolated as they are components of the two-dimensional surfaces. In order to emphasize this essential spatial feature of adsorption isotherms as a function of temperature and pressure, this work will use the adsorption isotherm surface to represent modeling results. For reader's convenience, the conventional adsorption isotherm curves and the extrapolating results for each individual adsorption isotherm are shown in *Supplementary Material*.

3 Results and discussion

3.1 Adsorption isotherm surface

Modelling results support the proposal that equation (4) simulates methane adsorption behavior in shales under test conditions very well as the RMSE (root of mean square error) is no larger than 0.002 as shown in Table 1.

Table 1 Fitting parameters (equation (4)) for different shales

Samples	n_{max} (mmol/g)	v_a (cm^3/g)	α	E_1 (kJ/mol)	E_2 (kJ/mol)	A_1 (MPa^{-1})	A_2 (MPa^{-1})	RMSE
FC-72	0.4291	0.0170	0.6812	21.375	13.726	0.000720	0.000443	0.0020
FC-66	0.3217	0.0129	0.3042	13.654	21.122	0.000460	0.000767	0.0016
FC-47	0.3442	0.0133	0.1990	10.000	21.776	0.000868	0.000579	0.0011
Longmaxi	0.1727	0.0085	0.8595	33.435	10.000	9.77E-06	0.004061	0.0019

Both the predicted absolute adsorption surface and Gibbs excess adsorption surface are shown in Figure 3. These surfaces share the following characteristics: 1) the measured adsorption uptake increases to a maximum and then decreases as a function of gas pressure, 2) the crossover of measured adsorption isotherms under different temperatures occurs for observed adsorption isotherms when the 2D surface is projected onto the adsorption uptake-pressure plane because of the cone shape of the 2D surface, 3) the predicted absolute adsorption uptake increases at elevated pressures, and 4) in all cases increase in temperature has a negative effect on absolute adsorption uptake for methane in shales. All these features agree with observed phenomena of supercritical gas adsorption in geomaterials, e.g., shale and coal (Weniger et al., 2010; Gasparik et al., 2015; Tang et al., 2016; Tian et al., 2016; Li et al., 2017; Zhou et al., 2018; Hu et al, 2018). Both the temperature- and pressure- dependent behaviour of the measured methane adsorption uptake in shales can be attributed to the nature of the adsorbed methane, and the density of adsorbed methane is a function of both the temperature and pressure as discussed in Section 3.2 later. The maximum phenomenon in the measured adsorption uptakes is the competition between the density of gaseous and adsorbed methane. The measured adsorption uptake is the product of the volume of the adsorbed phase and the difference between the density of the adsorbed and gaseous methane, shown in equation (2). It is worth pointing out that the model used in this work assumes that the average volume of the adsorbed layer of methane is constant, while the model in our previous work was based on the assumption that the density of the adsorbed phase is an unknown constant (Tang et al., 2016a). The maximum adsorption uptake is 0.1727 mmol/g for the Longmaxi shale, which is similar to the value obtained in previous work, 0.1715 mmol/g (Tang et al., 2016a). The present work therefore provides an alternative approach to model adsorption isotherms and interpret supercritical methane adsorption behavior. The unique feature of the adsorption isotherm surface is that it can be used

to extrapolate gas content under subsurface reservoir conditions as the adsorption isotherm is part of the adsorption surface.
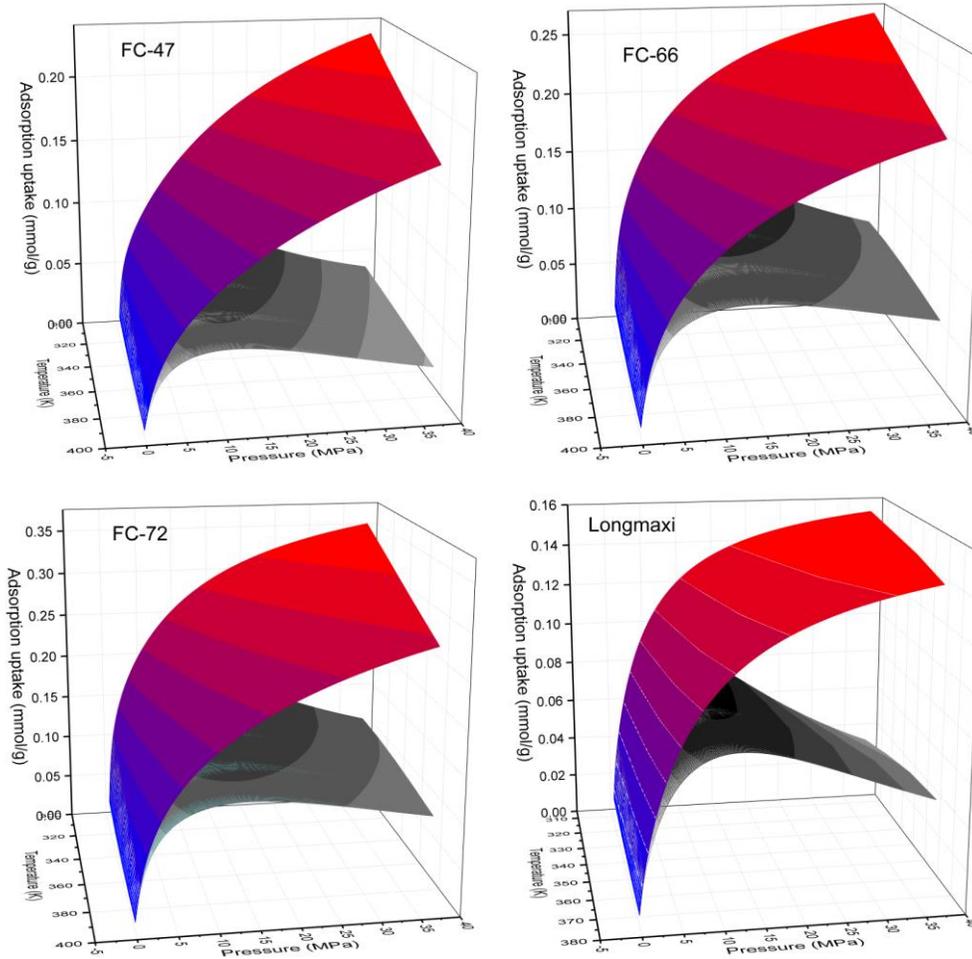

Figure 3 Supercritical methane adsorption isotherm surfaces in different shales under elevated pressures and temperatures: Blue to red colors represent predicted absolute adsorption surface, white to dark grey colors represent fitting surface of measured adsorption isotherms

3.2 Density of adsorbed phase of supercritical methane in shales

The density of the adsorbed phase of supercritical methane in shales as a function of pressure and temperature is shown in Figure 4. The density of the adsorbed methane follows a Langmuir type trend, which is always higher than the density of gaseous methane and always lower than liquid methane density (26.33 mmol/g). These results agree with current understanding of the adsorbed methane properties in porous media from MD simulations (Ambrose et al., 2010; Xiong et al., 2016; Tian et al., 2017; Zhang et al., 2014 & 2016; Liu et al., 2018; Li et al., 2014; Jin et al, 2013 & 2016; Zhu et al., 2014; Wu et al., 2015; Zhao et al., 2018). The differences in behavior of adsorbed methane density for the four shales can be attributed to their complex composition, pore structure and surface properties. Figure 4 also shows that the difference between adsorbed density and gaseous density first increases and then decreases with increasing pressures. This variation essentially determines the behavior of measured adsorption isotherms because the isotherms linearly increase with the density difference between adsorbed and gaseous phase when the volume of the adsorbed phase remains constant (equation (2)). Our proposed method

therefore provides another visualized interpretation for the observed behavior of measured adsorption isotherms, which rises to a maximum and then decreases with increasing pressures.
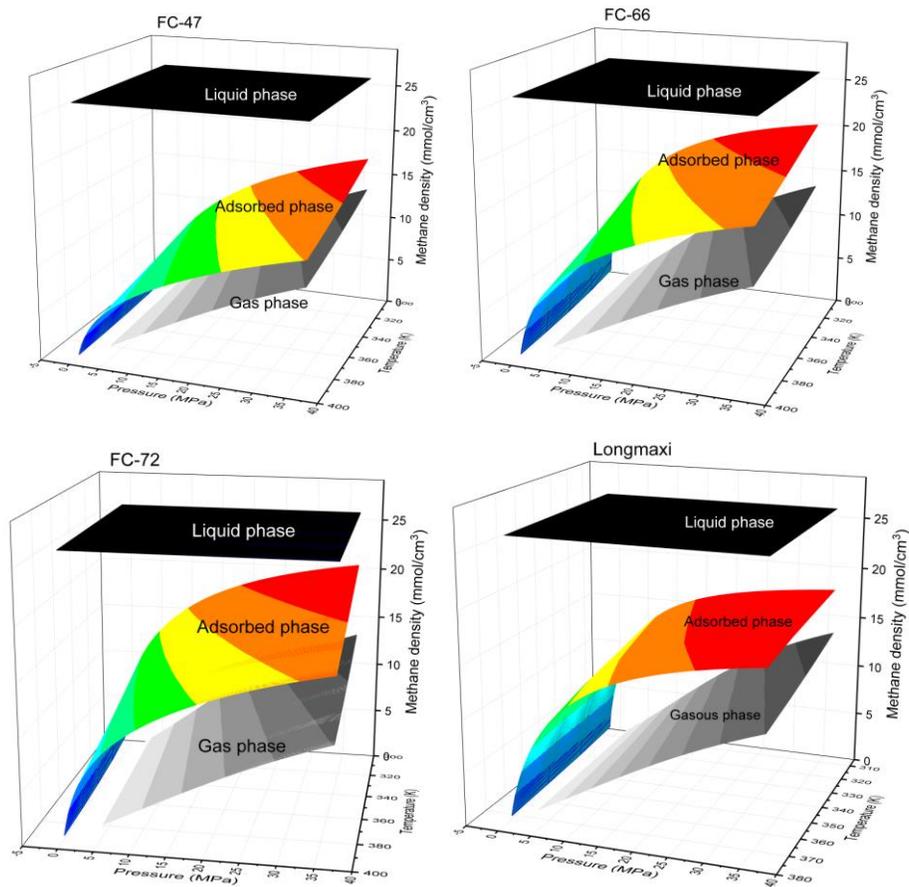

Figure 4. Density of adsorbed phase of supercritical methane in shales as a function of pressure and temperature: black horizontal surface represents the liquid methane density, colored surface represents the density of adsorbed phase, and the white to grey surface represents the density of gaseous methane obtained from REFPROP package.

3.3 Thermodynamic analysis

The calculated isosteric enthalpy of adsorption for methane in shale ranges from -8 kJ/mol to -30 kJ/mol as shown in Figure 5. The negative sign means the adsorption is an exothermic process, and the absolute value indicates methane adsorption in shales is a physical adsorption process. The calculated isosteric enthalpy of adsorption is found to be inversely dependent on temperature and the surface coverage (θ). This behavior is typical of gas adsorption on a heterogeneous surface where the adsorption sites are filled according to their energetic favorability. When the surface coverage is approaching saturation, the corresponding isosteric enthalpy increases slightly. The increasing isosteric enthalpy can be attributed to the strong adsorbate-adsorbate interactions when the adsorbed layer is approaching saturation. Temperature has a negative effect on isosteric enthalpy, and the higher the temperature the lower the isosteric enthalpy. When the surface coverage is less than 0.1, temperature can significantly influence the isosteric enthalpy. When the surface coverage is larger than 0.5, the isosteric enthalpy remains almost constant. The isosteric enthalpy as a function of surface coverage and temperature is a concave surface. The concave trend is similar to measured isosteric enthalpy for gas adsorption in porous

media using calorimetry (Dunne et al., 1996; Sircar et al., 1999; Terzyk et al.,1999; Shen et al., 2000; Giraldo et al, 2018; Moreno et al., 2018).
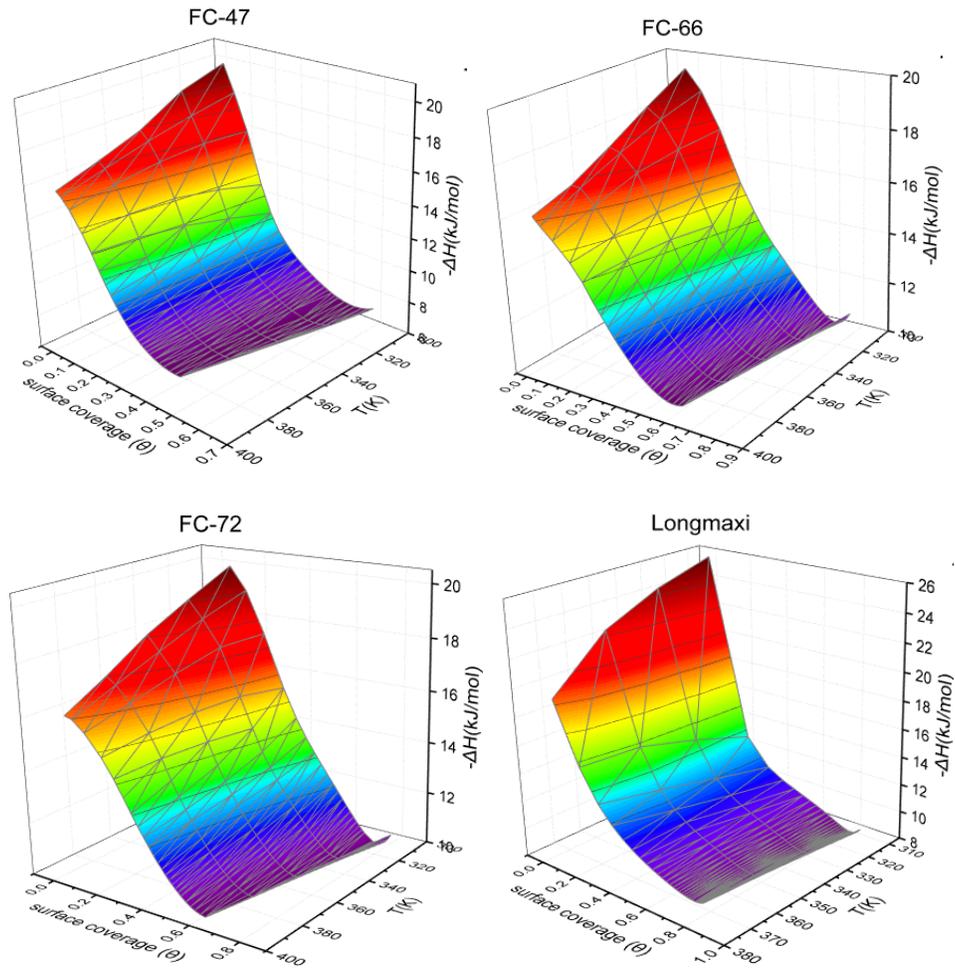

Figure 5. Isosteric enthalpy of adsorption as a function of temperature and surface coverage for methane in shales

The calculated isosteric entropy of adsorption for methane in shale ranges from -19 J/(mol K) to -70 J/(mol K) as shown in Figure 6. The negative entropy values indicate that the adsorption process is an enthalpy driven process. The calculated isosteric entropy of adsorption is also found to be dependent on temperature and the surface coverage (θ), and decreases with surface coverage increase. This is because when gas molecules are adsorbed, their freedom of movement becomes restricted. As temperature increases, the isosteric entropy decreases because the adsorbed phase is "less restricted" due to rise in temperature. It is worth emphasizing that the negative sign and the decreasing trend of the isoseric entropy does not violate the second law of thermodynamics as it states that the entropy of the universe always increases. This is because the entropy of the adsorption system does decrease but is more than compensated by the increase in the entropy of the surroundings due to the heat released during gas adsorption.
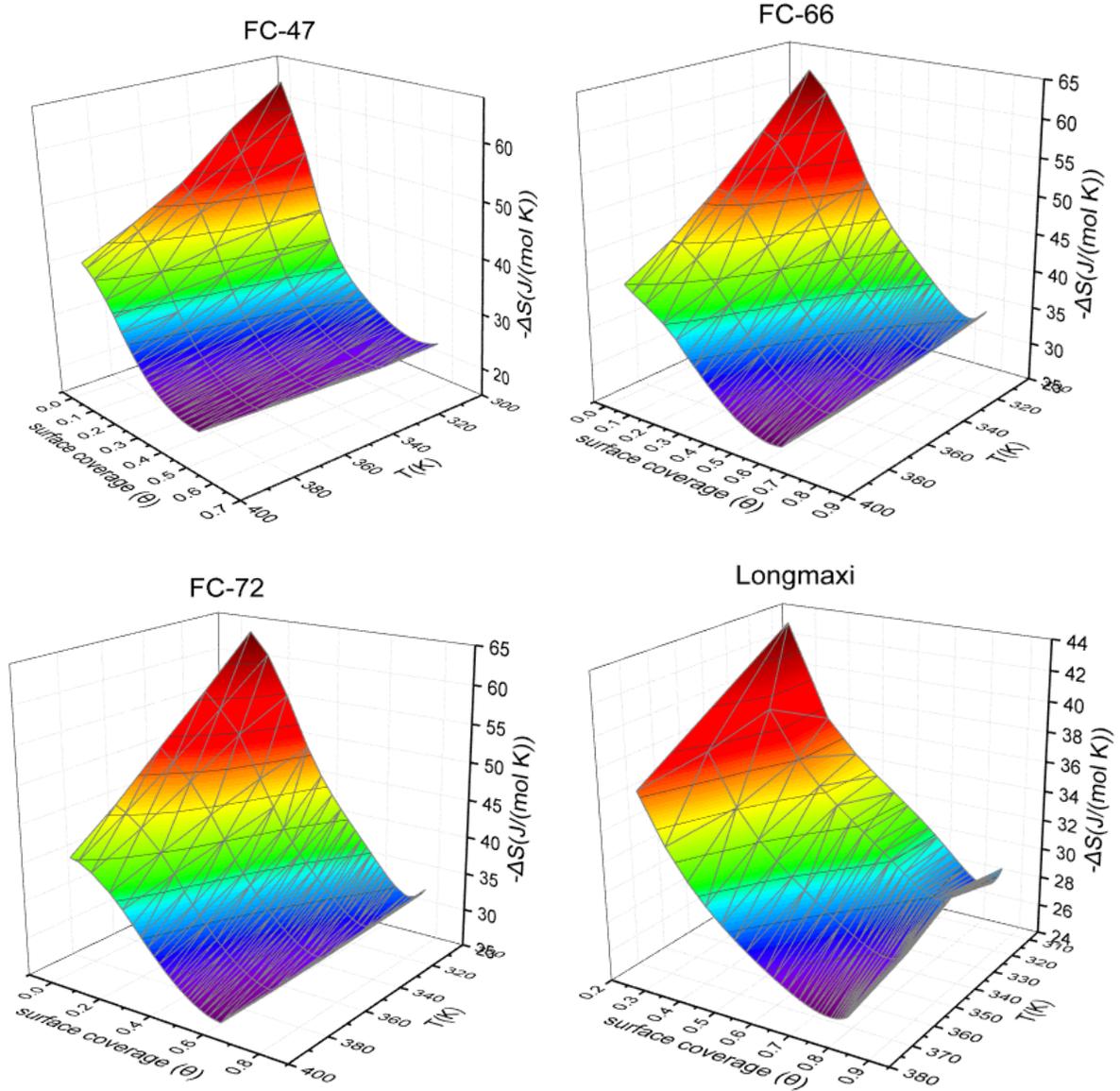
Figure 6. Isosteric entropy of adsorption as a function of temperature and surface coverage for methane in shales

3.4 Comparison with conventionally used method

To demonstrate the applicability of the proposed model, we compare our modeling results with those of two conventionally used methods, namely, the 3-parameter Langmuir model (eqs.12 & 13) and 3-parameter supercritical Dubinin–Radushkevich (SDR) model (eqs.14 & 15) (Li et al., 2017),

$$n_e = n_{max} \cdot \frac{K \cdot P}{1 + K \cdot P} \cdot (1 - \frac{\rho_g}{\rho_a}) \quad (12)$$

$$n_a = n_{max} \cdot \frac{K \cdot P}{1 + K \cdot P} \quad (13)$$

$$n_e = n_{max} \cdot \exp\{-D \cdot [\ln(\frac{\rho_a}{\rho_g}) \cdot R \cdot T]^2\} \cdot (1 - \frac{\rho_g}{\rho_a}) \quad (14)$$

$$n_a = n_{max} \cdot \exp\{-D \cdot [\ln(\frac{\rho_a}{\rho_g}) \cdot R \cdot T]^2\} \quad (15)$$

Where K is Langmuir constant, and D represents a pore structure parameter. For data processing, the unknown parameters, n_{max}, K and ρ_a in equation (12) and n_{max}, D and ρ_a in equation (14), can be obtained through fitting each measured adsorption isotherm independently using a curve fitting method such the least squares minimization (Tian et al, 2016; Rexer et al. 2013). The absolute adsorption uptake can then be obtained using equations (13) & (15). For thermodynamics potentials, the isosteric enthalpy (ΔH) and standard entropy (ΔS) are determined by a linear relationship ln(P) and 1/T at a specific absolute adsorption uptake. The term ln (0.1) is used for correcting the ΔS to the standard atmospheric pressure (0.1 MPa) (Li et al., 2017).

$$\ln(P)_{n_a} = -\frac{\Delta H}{R \cdot T} + \frac{R \cdot \ln(0.1) - \Delta S}{R} \quad (16)$$

It was demonstrated that both models fit the measured results very well, and details about the fitting performance and the corresponding results are shown in **Supplementary Material**. This section focuses on the comparison and interpretation of the modelling results from dual-site Langmuir, Langmuir and SDR model on maximum adsorption uptake, adsorbed methane density, absolute adsorption uptakes, and thermodynamic potentials.

Maximum adsorption uptake. It is generally accepted that the adsorption capacity of a shale is positively correlated to its total organic carbon (TOC) content (Zhang et al, 2012; Rexer et al., 2013; Gasparik et al., 2012; Weniger et al., 2010; Tian et al., 2016; Li et al., 2017; Zhou et al., 2018; Hu et al., 2018). The dual-site Langmuir model in Figure 7 shows this relationship, where the maximum adsorption uptake of shales increases with the increase of TOC. This can be attributed to the nature of the organic matter in shales, which is rich in nanopores and thus provides storage spaces for adsorbed methane. It is worthwhile to emphasize that the maximum adsorption uptake of shales in this work refers to the intrinsic adsorption capacity of shales, which is independent of test conditions and is determined by the pore structure and surface properties of the shale. The temperature- and pressure- dependent behavior of the adsorption isotherms solely relies on the adsorbed methane density as it is a function of temperature and pressure. Our interpretation here is different from the empirical maximum adsorption uptake of shales in most literature where equations. (12 & 14) are applied. The empirical maximum adsorption capacity is obtained by fitting each measured adsorption isotherm individually via different adsorption models, which show temperature- and pressure-dependent behavior (Zhang et al, 2012; Rexer et al., 2013; Gasparik et al., 2012; Weniger et al., 2010; Tian et al., 2016; Li et al., 2017; Zhou et al., 2018; Zou et al., 2017). In cases where researchers do not show the temperature-dependency of the empirical adsorption capacity (Tang et al., 2016b), the obtained indexes could be inaccurate because the temperature-dependent behavior contradicts with the assumptions of adsorption models. Most adsorption models, such as the classic Langmuir model and pore-filling models, assume that the adsorption sites or pore spaces do not change during adsorption (Langmuir, 1918; Dubinin, 1965, 1960 & 1971). Our framework therefore provides a new way to understand the temperature-dependent behavior of supercritical methane adsorption in shales and allows researchers to more accurately estimate gas resources in subsurface shale formations. It is worth to emphasize that the clay minerals in shale also have the capacity to adsorb methane and thus contribute the total methane adsorption uptake in shales (Ji et al., 2012; Fan et al., 2014; Heller et al, 2014 and Hwang et al, 2019), and more research works are needed to clarify the contribution of clay minerals for the maximum methane adsorption uptake in shales.
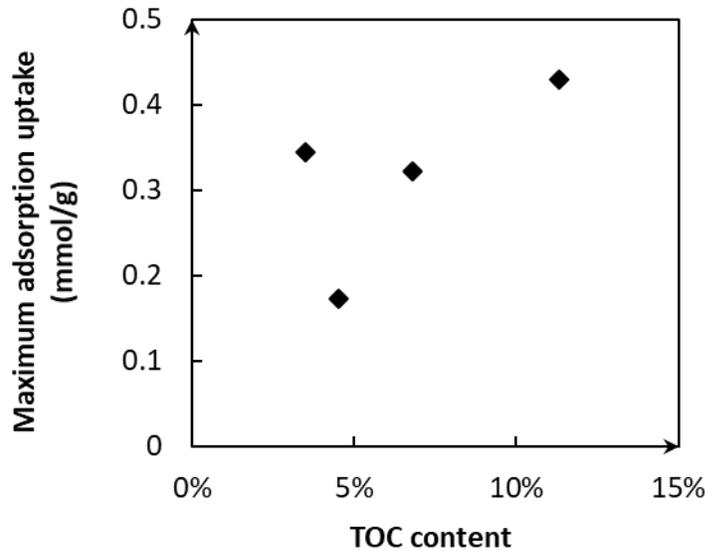
Figure 7 Relationship between maximum adsorption uptake of different shales and TOC

Adsorbed methane density. Since the equation of state for adsorbed methane is not measurable, developing alternative ways to estimate the density/volume of the adsorbed methane is key to understanding methane adsorption behavior in shales. Modelling results from the dual-site Langmuir model shows that the density of the adsorbed methane follows a Langmuir type trend, i.e., always higher than the density of gaseous methane and always lower than the density of liquid methane (Figure 4). These findings agree with the molecular dynamics in that the density of the adsorbed methane depends on both pressure and temperature (Tian et al., 2016; Rexer et al., 2013; Hu et al., 2018; Zhou et al., 2018). If both methods, i.e., equations (13) & (14), are adopted, one can obtain a constant density of adsorbed methane, which is independent of pressure and temperature. For the tested shale samples, the adsorbed methane density ranges from 18.89 mmol/cm^3 to 27.86 mmol/cm^3, and therefore some obtained values are higher than the density of liquid methane (26.33 mmol/cm^3).This contradicts the widely accepted fact that the adsorbed density is always lower than the liquid fluid density. Furthermore, this widely accepted method for modeling methane adsorption in shales is essentially inaccurate because the assumption of constant adsorbed density is suitable to a pore filling theory for vapor adsorption in microporous materials such as activated carbon and not for organic-rich shales containing both micropores (0-2nm) and mesopores (2-50 nm). Therefore, the dual-site Langmuir model provides an alternative way to model methane adsorption behavior in shales, which also allows researchers to probe the density of adsorbed methane in shales.

Absolute adsorption uptakes. Obtaining absolute adsorption uptake of methane in shales is fundamental for accurately estimating shale gas resources as well as understanding shale gas transport models in nanopores of shales. An incorrect ratio between adsorbed methane and gaseous methane for methane in shales was historically reported in literature because the absolute adsorption uptake and gaseous methane were estimated inaccurately (Tang et al. 2016a; Tang et al., 2017b). The absolute adsorption uptakes, extrapolated from measured data for our four shales using equations (3), (13) and (15), are shown in Figure 8. It was found that the absolute adsorption isotherm is a function of both temperature and pressure, and the absolute adsorption uptake is always higher than the corresponding experimentally obtained data. The absolute adsorption uptake from the dual-site Langmuir is much higher than that from the Langmuir and SDR model, which can be attributed to the constant density of adsorbed methane that comes from using equations (13) and (15) and a variable density of adsorbed methane using

equation (3). It is clear that using equations (13) and (15) underestimates the absolute adsorption uptakes. The results may imply that the absolute adsorption uptake, obtained using routinely applied methods, has been historically underestimated.
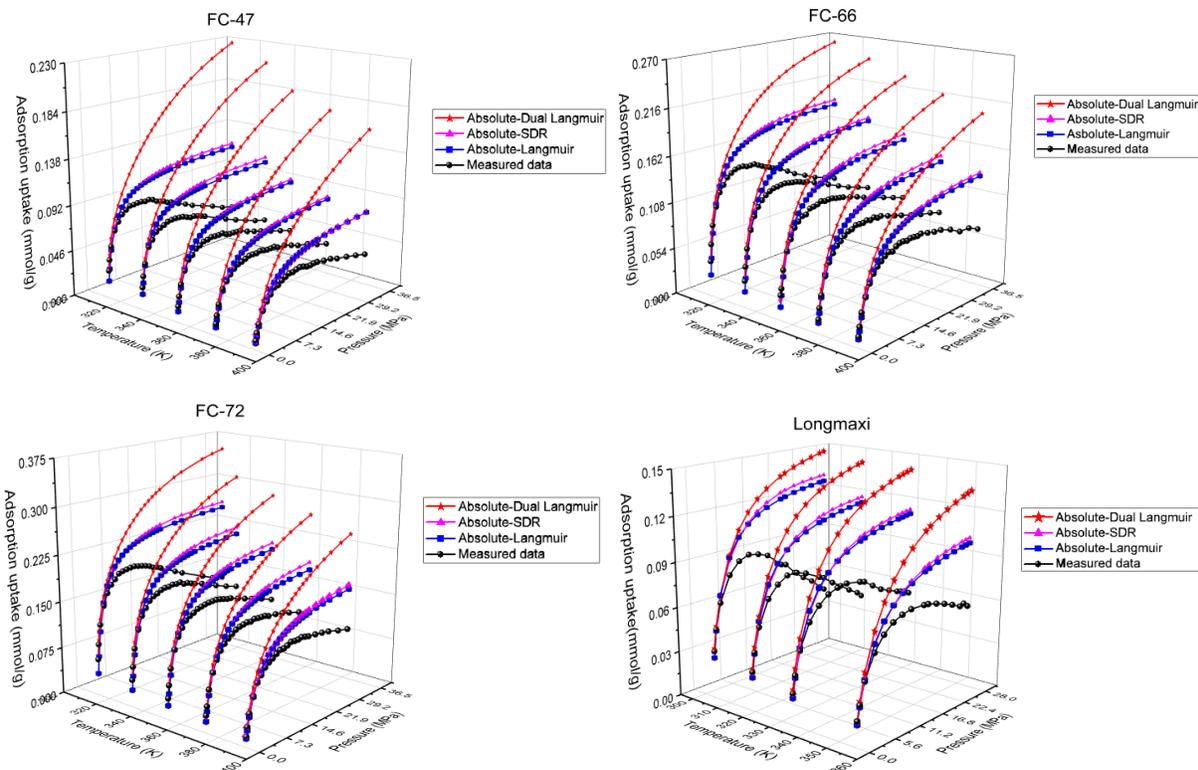

Figure 8. Absolute adsorption uptake of methane in different shales: dotted points represent data extrapolated from corresponding measured data, and lines are for guidance only.

Thermodynamic potentials. Thermodynamic potentials, such as isosteric enthalpy and entropy, indicate the interactions between gas molecules and shales. The isosteric enthalpy/entropy of adsorption calculated by the C-C equation through the curve fitting method (equation 15) has historically been used for describing the methane-shale interaction for different shales (Zhang et al., 2012; Gasparik et al., 2012; Rexer et al., 2013; Ji et al., 2015; Yang et al., 2015; Tian et al., 2016; Zou et al., 2017; Shabani et al., 2018; Li et al., 2018a; Li et al., 2018b). This method only gives a constant value of isosteric enthalpy/entropy for each adsorption isotherm, and the empirical relationship between temperature and isosteric enthalpy/entropy can also be obtained. For the tested shale samples, the isosteric enthalpy and entropy range from 21.8 kJ/mol to 22.2 kJ/mol and from 90.3 J/mol/K to 92.3 J/mol/K, respectively (Li et al., 2017). However, our work indicates that this conventional approach is inaccurate because it cannot consider non-ideal gas behavior and the contribution of the adsorbed phase because it applies the simplified form of C-C equation. The temperature-dependent behavior of the isosteric enthalpy is disclosed from these previous studies even though this behavior has been observed for gas adsorption in porous materials and by temperature measurement (Yue et al., 2015; Cao et al., 2001). The simplified form of C-C equation works well for dilute gas adsorption as ideal gas behavior is valid and the contribution of the adsorbed phase can be ignored. However, for supercritical gas adsorption, the C-C equation significantly overestimates the isosteric enthalpy as real gas behavior deviates from ideal gas law considerations and the volume of the adsorbed phase cannot be ignored. The isosteric enthalpy and entropy depends on surface coverage and temperature and are not constant for any one shale sample as shown in Figures 5 and 6. Therefore, both isosteric enthalpy

and entropy of methane adsorption in shales cannot be compared without specifying the corresponding surface coverage and temperatures, which was ignored in many previous studies (Zhang et al., 2012; Gasparik et al., 2012; Rexer et al., 2013; Ji et al., 2015; Yang et al., 2015; Tian et al., 2016; Zou et al., 2017; Shabani et al., 2018; Li et al., 2018a; Li et al., 2018b).

5 Conclusions

A rigorous framework to analyze adsorption equilibria for supercritical methane in shales has been developed in this report. This framework can accurately account for non-ideal gas properties and extrapolate absolute adsorption uptakes from measured adsorption isotherms. It allows accurate description of the complex behavior of thermodynamic indicators such as enthalpy and entropy relevant to adsorption. The modeling results were compared with results obtained using the routinely applied Langmuir model and supercritical Dubinin–Radushkevich (SDR) model. Our preliminary conclusions are as follows;

(1) The developed framework was successfully applied for describing supercritical methane adsorption isotherms (up to 32 MPa and 393.15 K) in four different shales. The measured and extrapolated adsorption isotherms in essence make up a two-dimensional adsorption isotherm surface. The developed adsorption isotherm surface can predict adsorption isotherms beyond experimentally obtained data.
(2) The maximum adsorption uptake of shale positively relates to the total organic carbon (TOC) content, which is determined by the material property of the shale and is independent of temperature. The higher the TOC, the larger the maximum adsorption uptake.
(3) The adsorbed methane density is found to be temperature- and surface coverage-dependent, and is higher the gaseous density but always lower than the density of liquid methane.
(4) The calculated isosteric enthalpy and entropy present the temperature- and surface coverage-dependent characteristics of supercritical methane in shales. In contrast, using the simplified Clausius–Clapeyron equation always overestimates the isosteric enthalpy and entropy and does not reveal the temperature-dependent characteristics.

Overall, the proposed framework lays the foundation for investigating supercritical fluid adsorption behavior in shales and the associated thermodynamics potentials. This method also allows analysis of how material properties of shales, such as composition, pore structure and surface chemistry, affect estimation of shale gas resources and associated thermodynamic potentials.

Supplementary Information

Acknowledgments

References

1. Ambrose, R. J., Hartman, R. C., Diaz Campos, M., Akkutlu, I. Y., & Sondergeld, C. (2010). New pore-scale considerations for shale gas in place calculations. In SPE Unconventional Gas Conference. Society of Petroleum Engineers.
2. Akkutlu, I. Y., & Fathi, E. (2012). Multiscale gas transport in shales with local kerogen heterogeneities. SPE journal, 17(04), 1-002.
3. Bae, J. S., & Bhatia, S. K. (2006). High-pressure adsorption of methane and carbon dioxide on coal. Energy & Fuels, 20(6), 2599-2607.
4. Cao, D. V., & Sircar, S. (2001). Temperature dependence of the isosteric heat of adsorption. Adsorption Science & Technology, 19(10), 887-894.
5. Chiang, W. S., Fratini, E., Baglioni, P., Chen, J. H., & Liu, Y. (2016). Pore size effect on methane adsorption in mesoporous silica materials studied by small-angle neutron scattering. Langmuir, 32(35), 8849-8857.
6. Chen, Y., Jiang, S., Zhang, D., & Liu, C. (2017). An adsorbed gas estimation model for shale gas reservoirs via statistical learning. Applied Energy, 197, 327-341.
7. Chakraborty, A., Saha, B. B., Koyama, S., & Ng, K. C. (2006). On the thermodynamic modeling of the isosteric heat of adsorption and comparison with experiments. Applied physics letters, 89(17), 171901.
8. Clausius, R. (1850), Ueber die bewegende Kraft der Wärme und die Gesetze, welche sich daraus für die Wärmelehre selbst ableiten lassen. Ann. Phys., 155: 500–524. doi:10.1002/andp.18501550403.
9. Clarkson, C. R., & Haghshenas, B. (2013). Modeling of supercritical fluid adsorption on organic-rich shales and coal. In SPE Unconventional Resources Conference-USA. Society of Petroleum Engineers.SPE164532.
10. Curtis, J. B. (2002). Fractured shale-gas systems. *AAPG bulletin*, *86*(11), 1921-1938.
11. Civan, F., Rai, C. S., & Sondergeld, C. H. (2011). Shale-gas permeability and diffusivity inferred by improved formulation of relevant retention and transport mechanisms. Transport in Porous Media, 86(3), 925-944.
12. Do, D. D., & Do, H. D. (2003). Adsorption of supercritical fluids in non-porous and porous carbons: analysis of adsorbed phase volume and density. Carbon, 41(9), 1777-1791.
13. Dubinin, M. (1965). Modern state of the theory of gas and vapour adsorption by microporous adsorbents. Pure and Applied Chemistry, 10(4), 309-322.
14. Dubinin, M. (1960). The potential theory of adsorption of gases and vapors for adsorbents with energetically nonuniform surfaces. Chemical Reviews, 60(2), 235-241.
15. Dubinin, M. M., & Astakhov, V. A. (1971). Development of the concepts of volume filling of micropores in the adsorption of gases and vapors by microporous adsorbents. Bulletin of the Academy of Sciences of the USSR, Division of chemical science, 20(1), 3-7.
16. Dunne, J. A., Rao, M., Sircar, S., Gorte, R. J., & Myers, A. L. (1996). Calorimetric heats of adsorption and adsorption isotherms. 2. O2, N2, Ar, CO2, CH4, C2H6, and SF6 on NaX, H-ZSM-5, and Na-ZSM-5 zeolites. Langmuir, 12(24), 5896-5904.
17. Gasparik, M., Ghanizadeh, A., Bertier, P., Gensterblum, Y., Bouw, S., & Krooss, B. M. (2012). High-pressure methane sorption isotherms of black shales from the Netherlands. Energy & fuels, 26(8), 4995-5004.
18. Gasparik, M., Gensterblum, Y., Ghanizadeh, A., Weniger, P., & Krooss, B. M. (2015). High-pressure/high-temperature methane-sorption measurements on carbonaceous shales by the manometric method: experimental and data-evaluation considerations for improved accuracy. SPE Journal, 20(04), 790-809.
19. Gensterblum, Y., Merkel, A., Busch, A., & Krooss, B. M. (2013). High-pressure CH4 and CO2 sorption isotherms as a function of coal maturity and the influence of moisture. International Journal of Coal Geology, 118, 45-57.

20. Gibbs, J. W. (1878). On the equilibrium of heterogeneous substances. American Journal of Science, (96), 441-458.
21. Giraldo, L., Rodriguez-Estupiñan, P., & Moreno-Piraján, J. C. (2018). A microcalorimetric study of methane adsorption on activated carbons obtained from mangosteen peel at different conditions. Journal of Thermal Analysis and Calorimetry, 132(1), 525-541.
22. Gor, G. Y., Huber, P., & Bernstein, N. (2017). Adsorption-induced deformation of nanoporous materials—A review. Applied Physics Reviews, 4(1), 011303.
23. Graham D. The characterization of physical adsorption systems. I. The equilibrium function and standard free energy of adsorption. J Phys Chem 1953;57(7):665–9.
24. Fan, E., Tang, S., Zhang, C., Guo, Q., & Sun, C. (2014). Methane sorption capacity of organics and clays in high-over matured shale-gas systems. Energy Exploration & Exploitation, 32(6), 927-942.
25. Heller, R., & Zoback, M. (2014). Adsorption of methane and carbon dioxide on gas shale and pure mineral samples. Journal of Unconventional Oil and Gas Resources, 8, 14-24.
26. Hwang, J., Joss, L., & Pini, R. (2019). Measuring and modelling supercritical adsorption of CO2 and CH4 on montmorillonite source clay. Microporous and Mesoporous Materials, 273, 107-121.
27. Huang, Y. Y. (1972). The temperature dependence of isosteric heat of adsorption on the heterogeneous surface. Journal of Catalysis, 25(1), 131-138.
28. Hu, H., Hao, F., Guo, X., Dai, F., Lu, Y., & Ma, Y. (2018). Investigation of methane sorption of overmature Wufeng-Longmaxi shale in the Jiaoshiba area, Eastern Sichuan Basin, China. Marine and Petroleum Geology, 91:251-261.
29. Jarvie, D. M., Hill, R. J., Ruble, T. E., & Pollastro, R. M. (2007). Unconventional shale-gas systems: The Mississippian Barnett Shale of north-central Texas as one model for thermogenic shale-gas assessment. AAPG bulletin, 91(4), 475-499.
30. Ji, W., Song, Y., Jiang, Z., Chen, L., Li, Z., Yang, X., & Meng, M. (2015). Estimation of marine shale methane adsorption capacity based on experimental investigations of Lower Silurian Longmaxi formation in the Upper Yangtze Platform, south China. Marine and Petroleum Geology, 68, 94-106.
31. Ji, L., Zhang, T., Milliken, K. L., Qu, J., & Zhang, X. (2012). Experimental investigation of main controls to methane adsorption in clay-rich rocks. Applied Geochemistry, 27(12), 2533-2545.
32. Jin, Z., & Firoozabadi, A. (2016). Phase behavior and flow in shale nanopores from molecular simulations. Fluid Phase Equilibria, 430, 156-168.
33. Jin, Z., & Firoozabadi, A. (2013). Methane and carbon dioxide adsorption in clay-like slit pores by Monte Carlo simulations. Fluid Phase Equilibria, 360, 456-465.
34. Kargbo, D. M., Wilhelm, R. G., & Campbell, D. J. (2010). Natural gas plays in the Marcellus Shale: Challenges and potential opportunities. Environ. Sci. Technol.,44 (15), pp 5679–5684.
35. Langmuir, I. (1918). The adsorption of gases on plane surfaces of glass, mica and platinum. Journal of the American Chemical society, 40(9), 1361-1403.
36. Lemmon, E. W., Huber, M. L., & McLinden, M. O. (2007). Reference fluid thermodynamic and transport properties–REFPROP Version 8.0. NIST standard reference database, 23.
37. Li, T., Tian, H., Xiao, X., Cheng, P., Zhou, Q., & Wei, Q. (2017). Geochemical characterization and methane adsorption capacity of overmature organic-rich Lower Cambrian shales in northeast Guizhou region, southwest China. Marine and Petroleum Geology, 86, 858-873.
38. Li, J., Zhou, S., Gaus, G., Li, Y., Ma, Y., Chen, K., & Zhang, Y. (2018a). Characterization of methane adsorption on shale and isolated kerogen from the Sichuan Basin under

pressure up to 60 MPa: Experimental results and geological implications. International Journal of Coal Geology, 189, 83-93.

39. Li, J., Chen, Z., Wu, K., Wang, K., Luo, J., Feng, D., ... & Li, X. (2018b). A multi-site model to determine supercritical methane adsorption in energetically heterogeneous shales. Chemical Engineering Journal, 349, 438-455.

40. Liu, Y., Li, H. A., Tian, Y., Jin, Z., & Deng, H. (2018). Determination of the absolute adsorption/desorption isotherms of CH 4 and n-C 4 H 10 on shale from a nano-scale perspective. Fuel, 218, 67-77.

41. Li, Z., Jin, Z., & Firoozabadi, A. (2014). Phase behavior and adsorption of pure substances and mixtures and characterization in nanopore structures by density functional theory. SPE Journal, 19(06), 1-096.

42. Loucks, R. G., Reed, R. M., Ruppel, S. C., & Jarvie, D. M. (2009). Morphology, genesis, and distribution of nanometer-scale pores in siliceous mudstones of the Mississippian Barnett Shale. Journal of sedimentary research, 79(12), 848-861.

43. Marmur, A. (2015). Surface tension and adsorption without a dividing surface. Langmuir, 31(46), 12653-12657.

44. McGlade, C., Speirs, J., & Sorrell, S. (2013). Methods of estimating shale gas resources– Comparison, evaluation and implications. Energy, 59, 116-125.

45. McHugh, M., & Krukonis, V. (2013). Supercritical fluid extraction: principles and practice. Elsevier.

46. Mertens, F. O. (2009). Determination of absolute adsorption in highly ordered porous media. Surface Science, 603(10), 1979-1984.

47. Moreno-Piraján, J. C., Bastidas-Barranco, M. J., & Giraldo, L. (2018). Preparation of activated carbons for storage of methane and its study by adsorption calorimetry. Journal of Thermal Analysis and Calorimetry, 131(1), 259-271.

48. Murata, K., El-Merraoui, M., & Kaneko, K. (2001). A new determination method of absolute adsorption isotherm of supercritical gases under high pressure with a special relevance to density-functional theory study. The Journal of Chemical Physics, 114(9), 4196-4205.

49. Murialdo, M., Ahn, C. C., & Fultz, B. (2018). A thermodynamic investigation of adsorbate-adsorbate interactions of carbon dioxide on nanostructured carbons. AIChE Journal, 64(3), 1026-1033.

50. Pan, H., Ritter, J. A., & Balbuena, P. B. (1998). Examination of the approximations used in determining the isosteric heat of adsorption from the Clausius-Clapeyron equation. Langmuir, 14(21), 6323-6327.

51. Pini, R., Ottiger, S., Burlini, L., Storti, G., & Mazzotti, M. (2010). Sorption of carbon dioxide, methane and nitrogen in dry coals at high pressure and moderate temperature. International Journal of Greenhouse Gas Control, 4(1), 90-101.

52. Pini, R. (2014). Interpretation of net and excess adsorption isotherms in microporous adsorbents. Microporous and Mesoporous Materials, 187, 40-52.

53. Rexer, T. F., Benham, M. J., Aplin, A. C., & Thomas, K. M. (2013). Methane adsorption on shale under simulated geological temperature and pressure conditions. Energy & Fuels, 27(6), 3099-3109.

54. Ross, D. J., & Bustin, R. M. (2009). The importance of shale composition and pore structure upon gas storage potential of shale gas reservoirs. Marine and Petroleum Geology, 26(6), 916-927.

55. Thommes, M., Kaneko, K., Neimark, A. V., Olivier, J. P., Rodriguez-Reinoso, F., Rouquerol, J., & Sing, K. S. (2015). Physisorption of gases, with special reference to the evaluation of surface area and pore size distribution (IUPAC Technical Report). Pure and Applied Chemistry, 87(9-10), 1051-1069.

56. Sakurovs, R., Day, S., Weir, S., & Duffy, G. (2007). Application of a modified Dubinin-Radushkevich equation to adsorption of gases by coals under supercritical conditions. Energy & fuels, 21(2), 992-997.
57. Slatt, R. M., & O'Brien, N. R. (2011). Pore types in the Barnett and Woodford gas shales: Contribution to understanding gas storage and migration pathways in fine-grained rocks. AAPG bulletin, 95(12), 2017-2030.
58. Shabani, M., Moallemi, S. A., Krooss, B. M., Amann-Hildenbrand, A., Zamani-Pozveh, Z., Ghalavand, H., & Littke, R. (2018). Methane sorption and storage characteristics of organic-rich carbonaceous rocks, Lurestan province, southwest Iran. International Journal of Coal Geology, 186, 51-64.
59. Shen, D., Bülow, M., Siperstein, F., Engelhard, M., & Myers, A. L. (2000). Comparison of experimental techniques for measuring isosteric heat of adsorption. Adsorption, 6(4), 275-286.
60. Sircar, S., Mohr, R., Ristic, C., & Rao, M. B. (1999). Isosteric heat of adsorption: theory and experiment. The Journal of Physical Chemistry B, 103(31), 6539-6546.
61. Sondergeld, C. H., Newsham, K. E., Comisky, J. T., Rice, M. C., & Rai, C. S. (2010, January). Petrophysical considerations in evaluating and producing shale gas resources. In SPE Unconventional Gas Conference. Society of Petroleum Engineers.
62. Stadie, N. P., Murialdo, M., Ahn, C. C., & Fultz, B. (2013). Anomalous isosteric enthalpy of adsorption of methane on zeolite-templated carbon. Journal of the American Chemical Society, 135(3), 990-993.
63. Stadie, N. P., Murialdo, M., Ahn, C. C., & Fultz, B. (2015). Unusual Entropy of Adsorbed Methane on Zeolite-Templated Carbon. The Journal of Physical Chemistry C, 119(47), 26409-26421.
64. Striolo, A., & Cole, D. R. (2017). Understanding shale gas: Recent progress and remaining challenges. Energy & Fuels, 31(10), 10300-10310.
65. Tang, X., Ripepi, N., Stadie, N. P., Yu, L., & Hall, M. R. (2016a). A dual-site Langmuir equation for accurate estimation of high pressure deep shale gas resources. Fuel, 185, 10-17.
66. Tang, X., Ripepi, N. (2016b) Temperature-dependent Langmuir model in the coal and methane sorption process: Statistical relationship, Transactions of the Society for Mining, Metallurgy & Exploration, 340: 61-19.
67. Tang, X., Ripepi, N., Stadie, N. P., & Yu, L. (2017a). Thermodynamic analysis of high pressure methane adsorption in Longmaxi shale. Fuel, 193, 411-418.
68. Tang, X., Ripepi, N., Luxbacher, K., & Pitcher, E. (2017b). Adsorption models for methane in shales: review, comparison and application. Energy & Fuels, 31 (10), 10787–10801.
69. Tang, X., & Ripepi, N. (2017c). High pressure supercritical carbon dioxide adsorption in coal: Adsorption model and thermodynamic characteristics. Journal of CO2 Utilization, 18, 189-197.
70. Tang, X. (2019). Surface thermodynamics of hydrocarbon vapors and carbon dioxide adsorption on shales. Fuel, 238, 402-411.
71. Terzyk, A. P., & Rychlicki, G. (1999). Calorimetric Investigations of Molecular Interactions in the Adsorbate/Microporous Activated Carbon System. Towards the Mechanism of Adsorption in Micropores. Adsorption Science & Technology, 17(5), 323-373.
72. Tian, H., Li, T., Zhang, T., & Xiao, X. (2016). Characterization of methane adsorption on overmature Lower Silurian–Upper Ordovician shales in Sichuan Basin, southwest China: Experimental results and geological implications. International Journal of Coal Geology, 156, 36-49.

73. Tian, Y., Yan, C., & Jin, Z. (2017). Characterization of Methane Excess and Absolute Adsorption in Various Clay Nanopores from Molecular Simulation. Scientific reports, 7(1), 12040.
74. Wang, Z., & Tang, X. (2018). New Insights from Supercritical Methane Adsorption in Coal: Gas Resource Estimation, Thermodynamics, and Engineering Application. Energy & Fuels, 32(4), 5001-5009.
75. Wang, S., Feng, Q., Zha, M., Javadpour, F., & Hu, Q. (2017). Supercritical methane diffusion in shale nanopores: effects of pressure, mineral types, and moisture content. Energy & fuels, 32(1), 169-180.
76. Wang, T., Tian, S., Li, G., Sheng, M., Ren, W., Liu, Q., & Zhang, S. (2018). Molecular simulation of CO2/CH4 competitive adsorption on shale kerogen for CO2 sequestration and enhanced gas recovery. The Journal of Physical Chemistry C, 122(30), 17009-17018.
77. Wang, S., Feng, Q., Javadpour, F., Hu, Q., & Wu, K. (2019). Competitive adsorption of methane and ethane in montmorillonite nanopores of shale at supercritical conditions: A grand canonical Monte Carlo simulation study. Chemical Engineering Journal, 355, 76-90.
78. Weniger, P., Kalkreuth, W., Busch, A., & Kroos, B. M. (2010). High-pressure methane and carbon dioxide sorption on coal and shale samples from the Paraná Basin, Brazil. International Journal of Coal Geology, 84(3), 190-205.
79. Wu, H., Chen, J., & Liu, H. (2015). Molecular dynamics simulations about adsorption and displacement of methane in carbon nanochannels. The Journal of Physical Chemistry C, 119(24), 13652-13657.
80. Xiong, J., Liu, K., Liu, X., Liang, L., & Zeng, Q. (2016). Molecular simulation of methane adsorption in slit-like quartz pores. RSC Advances, 6(112), 110808-110819.
81. Yang, F., Ning, Z., Zhang, R., Zhao, H., & Kroos, B. M. (2015). Investigations on the methane sorption capacity of marine shales from Sichuan Basin, China. International Journal of Coal Geology, 146, 104-117.
82. Yue, G., Wang, Z., Tang, X., Li, H., & Xie, C. (2015). Physical simulation of temperature influence on methane sorption and kinetics in coal (II): temperature evolvement during methane adsorption in coal measurement and modeling. Energy & Fuels, 29(10), 6355-6362.
83. Zhang, J., Clennell, M. B., Dewhurst, D. N., & Liu, K. (2014). Combined Monte Carlo and molecular dynamics simulation of methane adsorption on dry and moist coal. Fuel, 122, 186-197.
84. Zhang, J., Clennell, M. B., Liu, K., Pervukhina, M., Chen, G., & Dewhurst, D. N. (2016). Methane and carbon dioxide adsorption on Illite. Energy & Fuels, 30(12), 10643-10652.
85. Zhang, T., Ellis, G. S., Ruppel, S. C., Milliken, K., & Yang, R. (2012). Effect of organic-matter type and thermal maturity on methane adsorption in shale-gas systems. Organic Geochemistry, 47, 120-131.
86. Zhao, H., Wu, T., & Firoozabadi, A. (2018). High pressure sorption of various hydrocarbons and carbon dioxide in Kimmeridge Blackstone and isolated kerogen. Fuel, 224, 412-423.
87. Zhou, L., Zhou, Y., Li, M., Chen, P., & Wang, Y. (2000a). Experimental and modeling study of the adsorption of supercritical methane on a high surface activated carbon. Langmuir, 16(14), 5955-5959.
88. Zhou, L., Li, M., & Zhou, Y. (2000b). Measurement and theoretical analysis of the adsorption of supercritical methane on superactivated carbon. Science in China Series B: Chemistry, 43(2), 143-153.
89. Zhou, Y., & Zhou, L. (2009). Fundamentals of high pressure adsorption. Langmuir, 25(23), 13461-13466.

90. Zhou, S., Xue, H., Ning, Y., Guo, W., & Zhang, Q. (2018). Experimental study of supercritical methane adsorption in Longmaxi shale: Insights into the density of adsorbed methane. Fuel, 211, 140-148.
91. Zhu, X., & Zhao, Y. P. (2014). Atomic mechanisms and equation of state of methane adsorption in carbon nanopores. The Journal of Physical Chemistry C, 118(31), 17737-17744.
92. Zou, J., Rezaee, R., & Liu, K. (2017). Effect of Temperature on Methane Adsorption in Shale Gas Reservoirs. Energy & Fuels, 31(11), 12081-12092.